# Coherent Exciton Dynamics in Supramolecular Light-Harvesting Nanotubes Revealed by Ultrafast Quantum Process Tomography

Joel Yuen-Zhou,[†] Dylan H. Arias,[†,‡] Dorthe M. Eisele,[†,‡] Colby P. Steiner,[†,‡] Jacob J. Krich,[§] Moungi G. Bawendi,[†,‡] Keith A. Nelson,[†,‡] and Alán Aspuru-Guzik[†,⊥],*

[†]Center for Excitonics, Research Laboratory of Electronics, Massachusetts Institute of Technology, Cambridge, Massachusetts, United States, [‡]Department of Chemistry, Massachusetts Institute of Technology, Cambridge, Massachusetts, United States, [§]Department of Physics, University of Ottawa, Ottawa, ON, Canada, and [⊥]Department of Chemistry and Chemical Biology, Harvard University, Cambridge, Massachusetts, United States

ABSTRACT Long-lived exciton coherences have been recently observed in photosynthetic complexes *via* ultrafast spectroscopy, opening exciting possibilities for the study and design of coherent exciton transport. Yet, ambiguity in the spectroscopic signals has led to arguments against interpreting them in terms of exciton dynamics, demanding more stringent tests. We propose a novel strategy, quantum process tomography (QPT), for ultrafast spectroscopy and apply it to reconstruct the evolving quantum state of excitons in double-walled supramolecular light-harvesting nanotubes at room temperature from eight narrowband transient grating experiments. Our analysis reveals the absence of nonsecular processes, unidirectional energy transfer from the outer to the inner wall exciton states, and coherence between those states lasting about 150 fs, indicating weak electronic coupling between the walls. Our work constitutes the first experimental QPT in a "warm" and complex system and provides an elegant scheme to maximize information from ultrafast spectroscopy experiments.
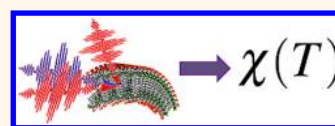
KEYWORDS: quantum process tomography · supramolecular aggregates · energy transfer · exciton coherence · ultrafast spectroscopy · open quantum system · nonlinear optics

Recently, there has been great excitement about the detection of long-lived coherent dynamics in natural light-harvesting photosynthetic complexes *via* two-dimensional spectroscopy.[1−3] This long-lived coherence has generated interest and debate about its role in the efficient design of light harvesters and exciton transport in biological and artificial settings.[4−7] These discussions have highlighted the importance of correctly interpreting the spectroscopic signals in terms of the microscopic dynamics in the material. The interplay between excitonic dynamics and vibrational dynamics can produce complex and potentially ambiguous spectroscopic signals, which can make extraction of information about exciton transport challenging.[8−10] Therefore, it is essential to develop methods to reliably extract the quantum dynamics of the interrogated material.[11,12] In this article, we demonstrate the complete and systematic characterization of room-temperature quantum dynamics of a condensed phase model

molecular system with a well-understood absorption spectrum[13,14] *via* ultrafast quantum process tomography (QPT);[15−18] we fully determine the dynamics of the excitons originating from the inner and outer walls of supramolecular light-harvesting nanotubes (Figure 1a). This article is organized as follows: First, we briefly sketch the QPT formalism as a general method to maximize information from a quantum system interacting with its environment. Then, we describe the optical setup and the nanotubes and explain how these two are suited for the QPT protocol. Finally, we present the experimental data and its analysis, yielding a full characterization of the quantum dynamics of the excitonic system. To our knowledge, this article constitutes the first experimental realization of QPT on a molecular system in condensed phase and provides general guidelines to adapt standard spectroscopic experiments to carry out QPT.
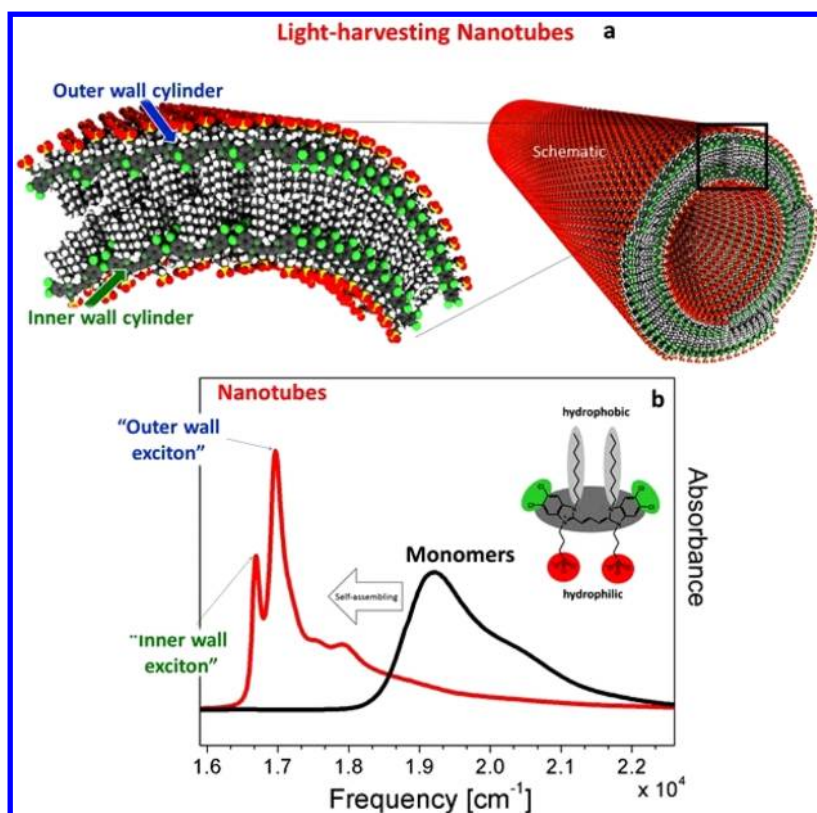
The time evolution of the excited state of an open quantum system (a system

Figure 1. The excitonic system under consideration: double-walled light-harvesting nanotube self-assembled from amphi-philic cyanine dye molecules. (a) Schematic of the double-walled nanotube (for clarity using only one molecule per unit cell) with the hydrophilic sulfonate groups (red) on the exterior, the hydrophobic alkyl chains (light gray) in the interior of the bilayer, and the cyanine dye chromophore (dark gray). (b) Absorption spectra of amphiphilic dye monomers C8S3 (black) dissolved in methanol (no aggregation) and nanotubular aggregates prepared in water/methanol (red). The nanotube's inner wall and outer wall cylinders featuring distinct delocalized exciton transitions associated with the $|I\rangle$ and $|O\rangle$ excitons.[14] (Reprinted with permission from Eisele, D. M., et al., Nat. Nanotechnol. 2009, 4, 658−663, and Nat. Chem. 2012, 4, 655−662. Copyright Nature Publishing Group.)

interacting with its environment, e.g., an electronic system interacting with an environment of vibrations) that is prepared by a pump pulse is, under general assumptions, given by[16−19]

$$\rho(T) = \chi(T)\, \rho(0) \qquad (1)$$

where $\rho(T)$ is the density matrix of the system at time T after the pump pulse, and the *process matrix* $\chi(T)$ is a propagator that relates input and output states. By introducing a basis, eq 1 reads $\rho_{qp}(T) = \Sigma_{ij}\chi_{qpij}(T)\, \rho_{ij}(0)$, where $\chi_{qpij}(T)$ denotes a transition probability ampli-tude of ending in state $|q\rangle\langle p|$ at time T having started in state $|i\rangle\langle j|$. In other words, $\chi(T)$ characterizes the transfer processes among populations (diagonal elements of ρ) and coherences (off-diagonal elements of ρ). This phenomenology is familiar in nonlinear spectro-scopy and can be discussed in terms of double-sided Feynman diagrams.[18,20−22] The process matrix $\chi(T)$ is a linear transformation of $\rho(0)$, which in turn yields the remarkable observation that, once $\chi(T)$ is given, the dynamics of the system are completely characterized; they are valid for arbitrary system initial states, including any interaction with the environment, whether char-acterized by Markovian or non-Markovian processes.

The reconstruction of $\chi(T)$ is the central goal of QPT, an essential step in the verification of quantum technologies[23−31] and dynamical models. Determin-ing $\chi(T)$ ensures that we have extracted the maximal amount of information possible about the excited-state dynamics. Previous theoretical work showed that selectively preparing and measuring a number of linearly independent initial states via laser excitation suffices to accomplish QPT.[16−18,32,33] Hence, QPT can in principle be realized with the tools of ultrafast spectroscopy by collecting a sufficient number of signals with varying frequency, polarization, and time delays.

RESULTS AND DISCUSSION

We study the exciton states of light-harvesting nanotubes (Figure 1a and Methods) that self-assemble in a water/methanol solution from the amphi-philic cyanine dye monomer 3,3′-bis(2-sulfopropyl)-5,5′, 6,6′-tetrachloro-1,1′-dioctylbenzimidacarbocyanine[34] (abbreviated as C8S3) at room temperature (298 K). The nanotubes are 13 ± 1 nm in diameter and several micrometers long and have a remarkably uniform supramolecular structure:[13] they are composed of
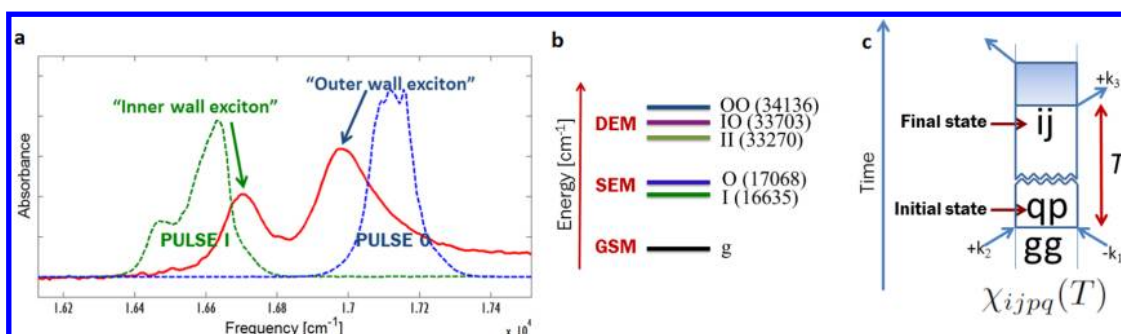
Figure 2. The concepts behind our QPT protocol. (a) Absorption spectrum of the light-harvesting nanotubes in the flow cell revealing only two optical transitions when exposed to light that is polarized along the long axes of the nanotubes. Each of the three pulses in each TG experiment is narrowband enough that it is selective toward the $\{|g\rangle \leftrightarrow |I\rangle, |I\rangle \leftrightarrow |II\rangle, |O\rangle \leftrightarrow |IO\rangle\}$ or the $\{|g\rangle \leftrightarrow |O\rangle, |O\rangle \leftrightarrow |OO\rangle, |I\rangle \rightarrow |IO\rangle\}$ transitions, respectively. **(b)** Energy level diagram of the system. Transitions are allowed between the ground-state manifold (GSM) and any state in the singly excited manifold (SEM) or between any state in the SEM and any in the doubly excited manifold (DEM). **(c)** Double-sided Feynman diagram representing the general idea of the QPT protocol using TG experiments. The first two pulses prepare the initial state, and the last two pulses detect the final state at the end of the waiting time T.

two concentric cylinders—an inner wall cylinder and an outer wall cylinder—separated by approximately 4 nm.[35,36]

Upon self-assembly, the broad absorption band of the monomer (Figure 1b) undergoes a large red-shift of $\sim$2500 cm^{-1}, reflecting the strong coupling of the molecules to form delocalized excitonic eigenstates.[37] In addition, a complex pattern of absorption bands occurs, caused by the nanotube's cylindrical geometry.[38,39] The two lowest energy bands correspond to transitions between the ground-state manifold (GSM) consisting of electronic state $|g\rangle$ and the singly excited manifold (SEM) consisting of electronic states $|I\rangle$ and $|O\rangle$, primarily originating from the inner wall and the outer wall cylinders, respectively.[14] These transitions occur at $\omega_{Ig} \approx 16\,600$ cm^{-1} and $\omega_{Og} \approx 17\,100$ cm^{-1} ($\omega_{ij} = \omega_i - \omega_j$ denotes a difference in energies) and are polarized primarily parallel to the cylindrical axis of the nanotubes, while the neighboring bands are mostly polarized in the equatorial plane. Flowing the nanotubes through a cell aligns their long axes with the direction of flow. Therefore, polarized light parallel to the flow can be used to isolate the transitions to $|I\rangle$ and $|O\rangle$, yielding the simplified absorption spectrum in Figure 2a. While the absorption spectrum of the nanotubes is well studied,[14] their excited-state dynamics are not fully understood. Therefore, they are an ideal candidate for ultrafast QPT on a condensed phase molecular system.

The well-separated peaks of $|I\rangle$ and $|O\rangle$ (Figure 1b) suggest a QPT scheme where selectivity is achievable by varying the carrier frequencies of the pulses and fixing their polarizations to be along the long axes of the nanotubes. In particular, we work within a transient grating (TG) setup, where three noncollinear narrowband beams with wavevectors k_1, k_2, and k_3 interact with the nanotubes. Beams 1 and 2 interact simultaneously ($t_1 = t_2$, where t_i denotes the arrival time of each pulse) with the nanotubes, creating a spatial grating from

which beam 3 is diffracted, generating a coherent signal with $k_s = -k_1 + k_2 + k_3$ that is detected using a fourth broadband reference pulse at $k_4 = k_s$ via spectral interferometry.[40] This generates a complex (absorptive and dispersive) spectrum as a function of waiting time $T = t_3 - t_2$ (see Methods). The first three narrowband pulses are chosen from a toolbox of two different pulse shapes, namely, a pulse that exclusively excites $|I\rangle$ and another one that excites $|O\rangle$, which we shall label as I and O, respectively. We then have eight different experiments associated with the triads of carrier frequencies: OOO, OOI, III, IIO, OIO, OII, IOI, and IOO. Figure 2a shows the spectra of the pulses on top of a magnified version of the absorption spectrum of the material from Figure 1b.

We are interested in probing the dynamics of the SEM with these optical experiments. In the TG experiment, the first two pulses prepare an initial SEM state.[17] This state evolves during the waiting time T, after which the third pulse probes the state by inducing stimulated emission (SE) to the GSM or excited state absorption (ESA) to the doubly excited manifold (DEM). The DEM consists of three electronic states with two excitons each: $|II\rangle$, $|IO\rangle$, and $|OO\rangle$, whose energies we assign as being the sums of the corresponding single-exciton states, with no binding energies, this being a reasonable assumption for molecular excitons (see Supporting Information, Sec. 2). We also detect the reduced absorption of the third pulse from the ground state $|g\rangle$ (due to the population moved to the SEM), known as ground-state bleach (GSB). Finally, the decay of this bleach is ground-state recovery (GSR), which contributes as the population in the SEM decays back to the GSM.

Figure 2b shows the energy level diagram for our system, as determined self-consistently from the TG spectra (see Supporting Information, Sec. 2). We implement our QPT scheme, illustrated in Figures 2c and 3, using the narrowband pulses I and O to selectively
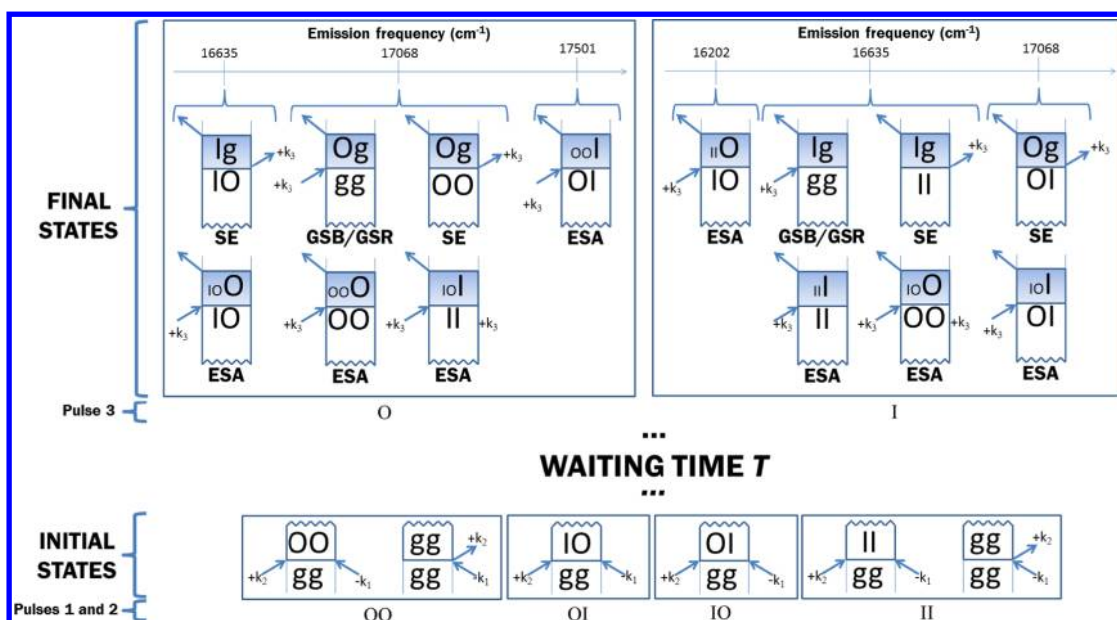
Figure 3. QPT protocol for the two-band exciton system of the double-walled nanotube. In the TG setup, the carrier frequencies of the first two narrowband pulses (bottom) selectively determine the possible initial states. Due to interactions with the vibrational surroundings (the bath), the initial state of the excitons can potentially transfer into other states of the SEM during the waiting time T. Narrowband pulse 3 and broadband reference pulse 4 detect these transfers by producing a frequency-resolved TG spectrum. The signals at each emission frequency give information on the state of the system at the end of the waiting time T.

prepare and detect populations or coherences in the SEM. Figure 3 exhaustively enumerates the possible initial states prepared by pulses 1 and 2 and the possible final states detected by pulses 3 and 4; together, these determine the elements of $\chi(T)$ that are measured at the indicated emission frequencies in the TG spectra. The emission frequencies are associated with the final elements in each Feynman diagram. For instance, let us consider the experiment OIO. Pulses 1 and 2 selectively prepare $\rho(0) = |I\rangle\langle O|$ (in the rotating wave approximation (RWA), pulse 1 "acts on the bra" and pulse 2 "acts on the ket")[20,22], and this state evolves for a time T. In a system with nonsecular dynamics, this coherence could induce a transfer to populations, producing nonzero probability amplitudes $\chi_{OOIO}(T)$ and $\chi_{IIIO}(T)$ of population being transferred into $|O\rangle\langle O|$ or $|I\rangle\langle I|$. These processes can be detected with the third pulse O, inducing the SE transition $|O\rangle\langle O| \rightarrow |O\rangle\langle g|$ and the ESA transitions $|O\rangle\langle O| \rightarrow |OO\rangle\langle O|$ and $|I\rangle\langle I| \rightarrow |IO\rangle\langle I|$, all of which emit at $\omega_{Og} = \omega_{OO,O} = \omega_{IO,I} = 17\,068\ \text{cm}^{-1}$ in the corresponding TG spectrum. If the initial coherence remains as $|I\rangle\langle O|$, then the third pulse O can induce SE to $|I\rangle\langle g|$ or ESA to $|IO\rangle\langle O|$, both producing signals at $\omega_{Og} = \omega_{IO,I} = 16\,635\ \text{cm}^{-1}$.

Figure 4 shows the data obtained from the eight frequency-resolved TG experiments as a function of waiting time T. The data for $T > 500$ fs were not included in the analysis due to the increasing influence of phase fluctuations in our pulse-shaping apparatus.[40] The below analysis indicates that the coherent dynamics are complete by 500 fs (see Figure 5). Both absorptive and dispersive (in our phase convention,

real and imaginary, respectively) parts of the complex-valued spectra are collected, but we show only the real part. Whereas Figure 3 predicts that three peaks in the frequency domain are possible in each of the spectra, we find that there is only one peak of significant amplitude in each spectrum, revealing that nonsecular processes such as coherence to population transfers are negligible or too small to be detected with the current experimental setup. Yet, as noted in the previous paragraph as well as in refs 9 and 16−18 and Supporting Information, Sec. 1, some of the peaks report on more than one element of $\chi(T)$, and a more careful procedure to dissect their contributions is necessary. In fact, each peak amplitude can be expressed as a linear combination of elements of $\chi(T)$ where the coefficients are products of transition dipole moments. We extract the required information about the dipoles self-consistently from the TG data via the initial condition that at $T = 0$ no transfer processes have occurred ($\chi_{ijqp}(0) = \delta_{iq}\delta_{jp}$; see Supporting Information, Sec. 2). The information associated with $\chi(T)$ is then obtained by integrating the area under the complex-valued peaks and carrying out a constrained linear inversion procedure. This procedure is a semidefinite programming routine[41,42] that ensures that the extracted $\chi(T)$ maps physical density matrices as inputs (Hermitian, trace preserving, and positive) to physical density matrices as outputs (Supporting Information, Sec. 3). We use the noise in each experiment at $T = 0$ at frequencies away from the strong emission frequencies to characterize the experimental uncertainties in the extracted dipoles; such uncertainties can be
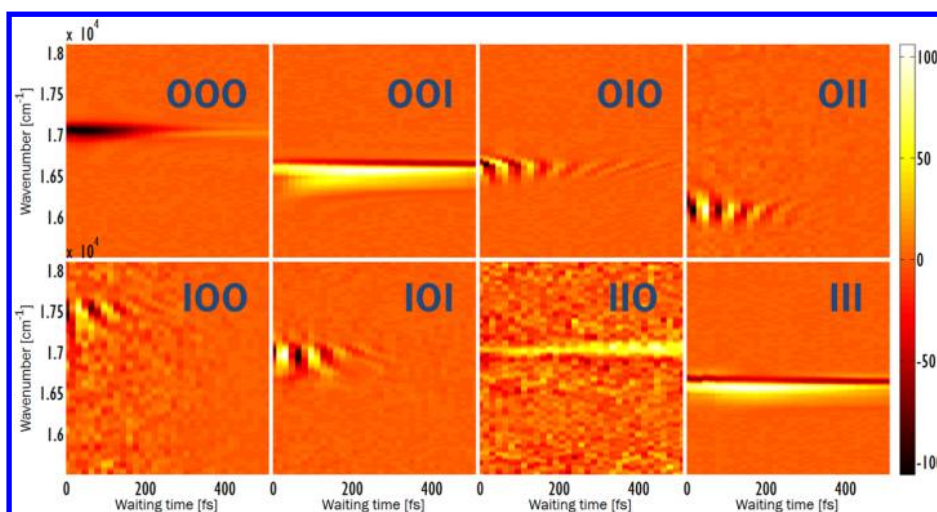
Figure 4. Absorptive part of eight narrowband TG experiments on the two-exciton-band system of the double-wall nanotube. The signals have been normalized to an arbitrary scale. The data show only one significant peak per spectrum (instead of a maximum of three, as outlined in Figure 3). Population transfer is revealed in the OOO, OOI, IIO, and III panels, whereas coherence dynamics are monitored by OIO, OII, IOO, and IOI. Coherence between $|I\rangle$ and $|O\rangle$ lasts for about 150 fs at room temperature and is observed as fringes as a function of waiting time T. The dispersive part of the data (not shown) exhibits qualitatively similar features.
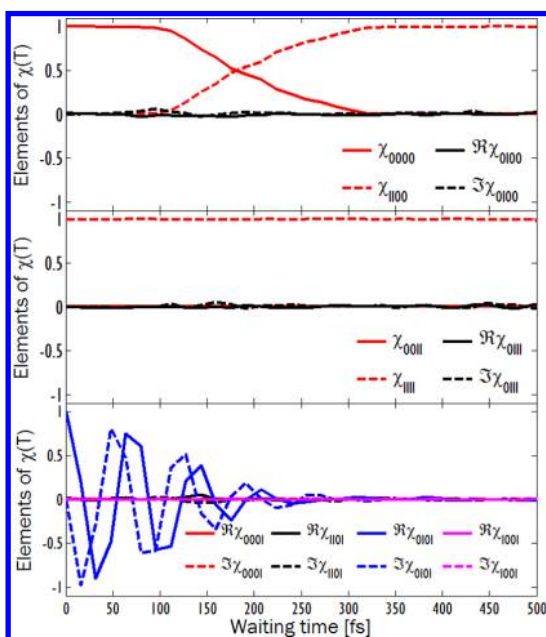
Figure 5. Nonzero elements of $\chi(T)$ extracted from the data of Figure 4. In the top panel, population transfer from the higher energy $|O\rangle$ to the lower energy $|I\rangle$ is monitored in the decay of $\chi_{OOOO}(T)$ and the rise of $\chi_{IIOO}(T)$ within the first 300 fs. In the center panel, no uphill transfer is observed from $|I\rangle$ to $|O\rangle$. Finally, the bottom panel shows secular coherence dynamics that last for about 150 fs, which indicates weak coupling between the I and O states.

reduced by increasing the signal-to-noise ratio. We use a Monte Carlo method to propagate these dipole uncertainties to uncertainties in the extracted fit parameters (Supporting Information, Sec. 3). The result of this numerical procedure is in Figure 5. Table 1 summarizes the values of the elements of $\chi(T)$ together with their time scales given by fits with 95% confidence intervals for the statistical error of the fit (first uncertainty) and for the propagated uncertainty in the dipoles (second uncertainty).

The full QPT analysis allows us to characterize all of the electronic processes occurring in the nanotubes' SEM. This single analysis gives complete information about the population transfer and coherence in the system. The results we find are consistent with previous experiments on similar systems (*e.g.*, for population and coherence times) but also unify them and allow unambiguous determination of energy transfer pathways. Figure 5 shows that, in this system, as anticipated, the nonsecular terms $\chi_{IOOO}(T)$, $\chi_{IOII}(T)$, $\chi_{IOOI}(T)$, $\chi_{IIOI}(T)$, and $\chi_{OOOI}(T)$ are negligible throughout the first 500 fs, indicating weak coupling between populations and coherences, as opposed to the situation of the Fenna–Matthews–Olson complex;[43] other analyses assume this result, but the QPT demonstrates it. On the other hand, $\chi_{OOOO}(T)$ and $\chi_{IIOO}(T)$ indicate that population from the higher energy $|O\rangle$ state transfers into $|I\rangle$ within 300 fs. Uphill transfer $|I\rangle \rightarrow |O\rangle$ is not observed, $\chi_{OOII}(T) \approx 0$ throughout the experiment, while the population term $\chi_{IIII}(T) \approx 1$ remains for all the times of interest. This analysis is distinctly different from other nonlinear spectroscopies, where the amount of collected information is insufficient to unambiguously separate uphill from downhill energy transfer pathways. We also explicitly track decay out of the SEM to the ground state g, $\chi_{ggqp}(T)$, and find all such decays to be negligible within the experiment, consistent with the reported time scales of radiative decay for supramolecular aggregates (on the order of tens to hundreds of picoseconds[44]); we can further conclude that there are no faster nonradiative pathways within the probed time scale. Similar conclusions were

TABLE 1. Time Scales of the Various Elements of $\chi(T)^a$

process	fit	description
$\chi_{0000}(T) \approx e^{-(T/\tau_{00})\beta_{00}}$	$\tau_{00} = 212 \pm 3 \pm 5$ fs, $\beta_{00} = 3.3 \pm 0.2 \pm 0.2$	population decay
$\chi_{II00}(T) \approx 1 - e^{-(T/\tau_{00})\beta_{00}}$	see above	population transfer
$\chi_{IIII}(T) \approx 1$ (>0.99)		population decay
$\chi_{00II}(T) \approx 0$ (<0.01)		population transfer
$\chi_{0I0I}(T) = \chi_{I0I0}^*(T) \approx e^{-i\omega_{0I}T} e^{-(T/\tau_{0I})\beta_{0I}}$	$2\pi/\omega_{0I} = 70 \pm 0.4 \pm 0.1$ fs,	decoherence
	$\tau_{0I} = 155 \pm 6 \pm 4$ fs, $\beta_{0I} = 2.6 \pm 0.3 \pm 0.2$	
$\chi_{I000}(T) = \chi_{0I00}^*(T), \chi_{I0II}(T) = \chi_{0III}^*(T), \chi_{\ I00I}(T) = \chi_{0II0}^*(T),$		nonsecular terms
$\chi_{\ II0I}(T) = \chi_{III0}^*(T), \chi_{000I}(T) = \chi_{00I0}^*(T) < 0.08$		

^{a} The non-negligible elements have been fit to the functional forms in the left column. The various kinetic parameters of these fits are listed in the center column. For each parameter, the first and second uncertainties refer to the fit and the uncertainty propagated from the transition dipoles, respectively (see Supporting Information Sec. 3). The right column classifies the elements of $\chi(T)$ into various physical processes.

observed in pump−probe[45] and two-dimensional spectra on a similar nanotubular system.[46] Finally, we detect an electronic coherence between $|O\rangle$ and $|I\rangle$ that decoheres after about 150 fs, allowing for a few quantum beats corresponding to $\omega_{0I} = 476$ cm^{-1} to appear. This beating indicates that the electronic coupling between the excitons in the two walls is on the same order as the coupling between these excitons and their respective vibrational baths. This type of electronic coupling was suggested in a similar nano-tubular system in the form of weak cross-peaks of the two-dimensional spectra, although quantum beats were not reported.[46] Such a weak coupling is consis-tent with previous redox chemistry experiments on this system.[14] The decoherence time scale is similar to reported values on a nanotube system with different chemical composition.[10,47−49] As shown in Table 1, the kinetics of the different processes in this system are characterized by stretched exponentials with indices β ranging between 2.6 and 3.3. We speculate that this is due to actual exponential kinetics embedded in Gaussian disorder, but more studies are needed to confirm this idea.

SUMMARY AND CONCLUSIONS

We have demonstrated for the first time the realiza-tion of QPT on a molecular system in condensed phase, namely, the inner and outer wall excitons of a supra-molecular light-harvesting nanotube. QPT has been obtained through the collection of a series of frequency-resolved TG spectra by systematically varying the frequency components of the pulses. *Via* numerical inversion of these signals, we have reconstructed the full process matrix $\chi(T)$ for the single-exciton dynamics. We summarize the main qualitative findings derived from the analysis of $\chi(T)$. First, an electronic coherence between the inner and outer wall excitons persists for more than a hundred femtoseconds, indicating a weak electronic coupling between the excitons originating from different walls. Second, population transfers uni-directionally from the outer to the inner wall exciton within the first hundreds of femtoseconds, consistent

with previous work on similar systems.[45,46] These transfers deviate from simple exponential kinetics, although this may be an effect of the ensemble measurements. Third, nonsecular relaxation dynamics are measured to be negligible, suggesting that the vibrational bath is dense and Markovian. These con-clusions are difficult to assess using a standard broad-band approach, where these processes are nontrivially convolved in a few peaks.[16−18] Instead, our QPT pro-tocol directly isolates each of these contributions in a systematic way.

As we have shown, QPT can be carried out by a straightforward adaptation of the traditional spectro-scopic experiment to ensure that the maximum amount of extractable information, at the quantum mechanical level, is obtained. QPT can be interpreted as a procedure that reconstructs the time-dependent quantum state of a system and, therefore, offers a systematic and transparent way to design ultrafast spectroscopy experiments. It complements the tradi-tional approach where only specific projections of the response of the material are collected and expands upon previous works, which can be regarded as partial QPT experiments.[11,12] The present article reports QPT on a model system with a well-understood absorption spectrum[14] and, therefore, constitutes a good demon-stration of the protocol for a SEM of dimension $d = 2$. For arbitrary dimensions, QPT requires on the order of d^4 data points per time T (see refs 17 and 18, SI-XII), which translates to about d^3 frequency-resolved TG spectra. If the collection of this amount of experimental data becomes formidable, it will be worth considering stochastic and compressed-sensing methods[52,53] or, alternatively, partial QPT protocols to pinpoint specific mechanisms that do not require the knowledge of an entire process matrix $\chi(T)$.

For future studies, we envision many opportunities where the QPT paradigm will be powerful in more complex materials. Specific examples include experi-ments on excitonic networks embedded in complex environments in biological[43] and solid-state systems,[50] or reactive molecular systems with strong vibronic

features,[51] where one expects an interesting interplay between electronic coherences and populations beyond secular dynamics and where the detailed imaging of the quantum dynamics is required in order to construct theoretical models. We foresee exciting opportunities in which the QPT approach to ultrafast spectroscopy will provide new insights into the excited-state dynamics of chemical systems.

METHODS

Synthesis of Supramolecular Light-Harvesting Nanotubes in Solution. The amphiphilic cyanine dye derivative 3,3′-bis(2-sulfopropyl)-5,5′,6,6′-tetrachloro-1,1′-dioctylbenzimidacarbocyanine (MW = 902.8 g mol^{-1}, Figure 1) was obtained as a sodium salt (FEW Chemicals) and used as received. The individual supramolecular light-harvesting nanotubes, consisting of concentric walls of excitons, were prepared in water/methanol as described in ref 13. Solutions of nanotubes were stored in the dark and used for experiments within 4 h. Absorption spectroscopy was used as a tool to monitor the aggregation process before and during the nonlinear spectroscopy experiments. We limited our investigation to samples that contained the expected spectral contributions from individual double-walled supramolecular light-harvesting nanotubes.[14]

Optical Methods. A noncollinear parametric amplifier[54] (NOPA) is pumped by a regeneratively amplified Ti:sapphire laser at 800 nm with a pulse energy of 350 μJ at a repetition rate of 10 kHz. The NOPA produces pulses with a central frequency of 16 800 cm^{-1}, full-width at half-maximum of 700 cm^{-1}, and approximately equal intensities at 16 600 and 17 100 cm^{-1}, i.e., the energies of the $|I\rangle$ and the $|O\rangle$ states. The pulses are compressed with a prism pair to approximately 20−25 fs.

After the NOPA, the beam passes through a 2D phase mask optimized for first-order diffraction to produce four beams in the BOXCARS geometry. The beams then enter a diffraction-based pulse shaper using a Hamamatsu X7550 2D spatial light modulator (SLM) for phase and amplitude shaping of the frequency components of each beam.[40] The beams are spectrally dispersed by a grating and imaged at different vertical positions by a cylindrical lens onto the SLM for independent temporal shaping. We apply a sawtooth grating pattern in the vertical dimension of the SLM device, enabling the amplitude of the frequency components of each beam to be controlled by the amplitude of the grating. In the experiments, a Gaussian amplitude filter is applied via SLM to each beam in order to diffract only the frequencies covering a single transition. Each broadband pulse has approximately 3.5 nJ/pulse, whereas the narrowband pulses have 450−500 pJ/pulse.

After pulse shaping, the beams are imaged onto the sample to perform a transient grating experiment. The first two narrowband pulses, with wavevectors k_1 and k_2, generate a spatially periodic excitation grating in the material due to the change in the refractive index upon excitation. The system is probed by the third narrowband pulse after a time delay. The third pulse, with wavevector k_3, diffracts off the grating into the TG direction, $k_s = -k_1 + k_2 + k_3$. The signal copropagates with the fourth beam, which acts as a (broadband) local oscillator for heterodyne detection. Spectral interferometry is used to retrieve both the real and imaginary parts of the signal. Between the collection of each of the eight TG spectra, a linear absorption measurement is obtained to ensure that the sample has not degraded.

Conflict of Interest: The authors declare no competing financial interest.

REFERENCES AND NOTES

1. Engel, G. S.; Calhoun, T. R.; Read, E. L.; Ahn, T. K.; Mancal, T.; Cheng, Y. C.; Blankenship, R. E.; Fleming, G. R. Evidence for Wavelike Energy Transfer through Quantum Coherence in Photosynthetic Systems. *Nature* **2007**, *446*, 782−786.
2. Collini, E.; Wong, C. Y.; Wilk, K. E.; Curmi, P. M. G.; Brumer, P.; Scholes, G. D. Coherently Wired Light-Harvesting in Photosynthetic Marine Algae at Ambient Temperature. *Nature* **2010**, *463*, 644−U69.
3. Panitchayangkoon, G.; Hayes, D.; Fransted, K. A.; Caram, J. R.; Harel, E.; Wen, J.; Blankenship, R. E.; Engel, G. S. Long-Lived Quantum Coherence in Photosynthetic Complexes at Physiological Temperature. *Proc. Natl. Acad. Sci. U.S.A.* **2010**, *107*, 12766−12770.
4. Mohseni, M.; Rebentrost, P.; Lloyd, S.; Aspuru-Guzik, A. Environment-Assisted Quantum Walks in Photosynthetic Energy Transfer. *J. Chem. Phys.* **2008**, *129*, 174106.
5. Plenio, M. B.; Huelga, S. F. Dephasing-Assisted Transport: Quantum Networks and Biomolecules. *New J. Phys.* **2008**, *10*, 113019.
6. Brumer, P.; Shapiro, M. Molecular Response in One-Photon Absorption via Natural Thermal Light vs. Pulsed Laser Excitation. *Proc. Nat. Acad. Sci.* **2012**, *109*, 19575−19578.
7. Kassal, I.; Yuen-Zhou, J.; Rahimi-Keshari, S. Does Coherence Enhance Transport in Photosynthesis? *J. Phys. Chem. Lett.* **2013**, *4*, 362−367.
8. Biggs, J. D.; Cina, J. A. Using Wave-Packet Interferometry to Monitor the External Vibrational Control of Electronic Excitation Transfer. *J. Chem. Phys.* **2009**, *131*, 224101.
9. Yuen-Zhou, J.; Krich, J. J.; Aspuru-Guzik, A. A Witness for Coherent Electronic vs. Vibronic-Only Oscillations in Ultrafast Spectroscopy. *J. Chem. Phys.* **2012**, *136*, 234501.
10. Milota, F.; Prokhorenko, V. I.; Mancal, T.; von Berlepsch, H.; Bixner, O.; Kauffmann, H. F.; Hauer, J. Vibronic and Vibrational Coherences in Two-Dimensional Electronic Spectra of Supramolecular J-Aggregates. *J. Phys. Chem. A* **2013**, *117*, 6007−6014.
11. Lee, H.; Cheng, Y. C.; Fleming, G. R. Coherence Dynamics in Photosynthesis: Protein Protection of Excitonic Coherence. *Science* **2007**, *316*, 1462−1465.
12. Richards, G. H.; Wilk, K. E.; Curmi, P. M. G.; Davis, J. A. Disentangling Electronic and Vibrational Coherence in the Phycocyanin-645 Light-Harvesting Complex. *J. Phys. Chem. Lett.* **2014**, *5*, 43−49.
13. Eisele, D. M.; Knoester, J.; Kirstein, S.; Rabe, J. P.; Bout, D. A. V. Uniform Exciton Fluorescence from Individual Molecular Nanotubes Immobilized on Solid Substrates. *Nat. Nanotechnol.* **2009**, 658−663.
14. Eisele, D. M.; Cone, C. W.; Bloemsma, E. A.; Vlaming, S. M.; van der Kwaak, C. G. F.; Silbey, R. J.; Bawendi, M. G.; Knoester, J.; Rabe, J. P.; Bout, D. A. V. Utilizing Redox-Chemistry to Elucidate the Nature of Exciton Transitions in Supramolecular Dye Nanotubes. *Nat. Chem.* **2012**, 655−662.
15. Rebentrost, P.; Shim, S.; Yuen-Zhou, J.; Aspuru-Guzik, A. Characterization and Quantification of the Role of Coherence in Ultrafast Quantum Biological Experiments Using Quantum Master Equations, Atomistic Simulations, and Quantum Process Tomography. *Procedia Chem.* **2011** *3*, 332.

16. Yuen-Zhou, J.; Aspuru-Guzik, A. Quantum Process Tomography of Excitonic Dimers from Two-Dimensional Electronic Spectroscopy. I. General Theory and Application to Homodimers. *J. Chem. Phys.* **2011**, *134*, 134505.

17. Yuen-Zhou, J.; Krich, J. J.; Mohseni, M.; Aspuru-Guzik, A. Quantum State and Process Tomography of Energy Transfer Systems *via* Ultrafast Spectroscopy. *Proc. Natl. Acad. Sci. U.S.A.* **2011**, *108*, 17615.

18. Yuen-Zhou, J.; Krich, J. J.; Kassal, I.; Johnson, A.; Aspuru-Guzik, A. *Ultrafast Spectroscopy: Quantum Information and Wavepackets*; Institute of Physics, 2014.

19. Nielsen, M. A.; Chuang, I. L. *Quantum Computation and Quantum Information*; Cambridge University Press, 2000.

20. Mukamel, S. *Principles of Nonlinear Optical Spectroscopy*; Oxford University Press, 1995.

21. Mukamel, S. Multidimensional Femtosecond Correlation Spectroscopies of Electronic and Vibrational Excitations. *Annu. Rev. Phys. Chem.* **2000**, *51*, 691–729.

22. Cho, M. *Two Dimensional Optical Spectroscopy*; CRC Press, 2009.

23. Riebe, M.; Kim, K.; Schindler, P.; Monz, T.; Schmidt, P. O.; Körber, T. K.; Hänsel, W.; Häffner, H.; Roos, C. F.; Blatt, R. Process Tomography of Ion Trap Quantum Gates. *Phys. Rev. Lett.* **2006**, *97*, 220407.

24. Childs, A. M.; Chuang, I. L.; Leung, D. W. Realization of Quantum Process Tomography in NMR. *Phys. Rev. A* **2001**, *64*, 012314.

25. Weinstein, Y. S.; Havel, T. F.; Emerson, J.; Boulant, N.; Saraceno, M.; Lloyd, S.; Cory, D. G. Quantum Process Tomography of the Quantum Fourier Transform. *J. Chem. Phys.* **2004**, *121*, 6117–6133.

26. Bialczak, R. C.; Ansmann, M.; Hofheinz, M.; Lucero, E.; Neeley, M.; O'Connell, A. D.; Sank, D.; Wang, H.; Wenner, J.; Steffen, M.; *et al*. Quantum Process Tomography of a Universal Entangling Gate Implemented with Josephson Phase Qubits. *Nat. Phys.* **2010**, *6*, 409–413.

27. Myrskog, S. H.; Fox, J. K.; Mitchell, M. W.; Steinberg, A. M. Quantum Process Tomography on Vibrational States of Atoms in an Optical Lattice. *Phys. Rev. A* **2005**, *72*, 013615.

28. Howard, M.; Twamley, J.; Wittmann, C.; Gaebel, T.; Jelezko, F.; Wrachtrup, J. Quantum Process Tomography and Linblad Estimation of a Solid-State Qubit. *New J. Phys.* **2006**, *8*, 33.

29. Branderhorst, M. P. A.; Nunn, J.; Walmsley, I. A.; Kosut, R. L. Simplified Quantum Process Tomography. *New J. Phys.* **2009**, *11*, 115010.

30. Humble, T. S.; Cina, J. A. Molecular State Reconstruction by Nonlinear Wave Packet Interferometry. *Phys. Rev. Lett.* **2004**, *93*, 060402.

31. Avisar, D.; Tannor, D. J. Complete Reconstruction of the Wave Function of a Reacting Molecule by Four-Wave Mixing Spectroscopy. *Phys. Rev. Lett.* **2011**, *106*, 170405.

32. Hoyer, S.; Whaley, K. B. Inverting Pump-Probe Spectroscopy for State Tomography of Excitonic Systems. *J. Chem. Phys.* **2013**, *138*, 164102.

33. de Castro, R. R.; Cabrera, R.; Bondar, D. I.; Rabitz, H. Time-Resolved Quantum Process Tomography Using Hamiltonian-Encoding and Observable-Decoding. *New J. Phys.* **2013**, *15*, 025032.

34. De Rossi, U.; Moll, J.; Spieles, M.; Bach, G.; Dahne, S.; Kriwanek, J.; Lisk, M. Control of the J-Aggregation Phenomenon by Variation of the N-Alkyl-Substituents. *J. Prak. Chem.-Chem. Ztg.* **1995**, *337*, 203–208.

35. von Berlepsch, H.; Kirstein, S.; Hania, R.; Pugzlys, A.; Bottcher, C. Modification of the Nanoscale Structure of the J-Aggregate of a Sulfonate-Substituted Amphiphilic Carbocyanine Dye through Incorporation of Surface-Active Additives. *J. Phys. Chem. B* **2007**, *111*, 1701–1711.

36. Eisele, D. M.; Berlepsch, H. v.; Bottcher, C.; Stevenson, K. J.; Vanden Bout, D. A.; Kirstein, S.; Rabe, J. P. Photoinitiated Growth of Sub-7 nm Silver Nanowires Within a Chemically Active Organic Nanotubular Template. *J. Am. Chem. Soc.* **2010**, *132*, 2104–2105.

37. Scholes, G. D.; Olaya-Castro, A.; Fleming, G. R.; van Grondelle, R. Lessons from Nature About Solar Light Harvesting. *Nat. Chem.* **2011**, 763–774.

38. Didraga, C.; Klugkist, J. A.; Knoester, J. Optical Properties of Helical Cylindrical Molecular Aggregates: The Homogeneous Limit. *J. Phys. Chem. B* **2002**, *106*, 11474–11486.

39. Didraga, C.; Pugzlys, A.; Hania, P. R.; von Berlepsch, H.; Duppen, K.; Knoester, J. Structure, Spectroscopy, and Microscopic Model of Tubular Carbocyanine Dye Aggregates. *J. Phys. Chem. B* **2004**, *108*, 14976–14985.

40. Turner, D.; Stone, K. W.; Gundogdu, K.; Nelson, K. A. The Coherent Optical Laser Beam Recombination Technique (COLBERT) Spectrometer: Coherent Multidimensional Spectroscopy Made Easier. *Rev. Sci. Instrum.* **2011**, *82*, 081301.

41. Grant, M.; Boyd, S. In *Recent Advances in Learning and Control*; Blondel, V., Boyd, S., Kimura, H., Eds.; Lecture Notes in Control and Information Sciences; Springer-Verlag Limited, 2008; pp 95−110.

42. Grant, M.; Boyd, S. *CVX: Matlab Software for Disciplined Convex Programming*, Version 1.21; 2011.

43. Panitchayangkoon, G.; Voronine, D. V.; Abramavicius, D.; Caram, J. R.; Lewis, N. H. C.; Mukamel, S.; Engel, G. S. Direct Evidence of Quantum Transport in Photosynthetic Light-Harvesting Complexes. *Proc. Natl. Acad. Sci. U.S.A.* **2011**, *108*, 20908–20912.

44. Moll, J.; Daehne, S.; Durrant, J. R.; Wiersma, D. A. Optical Dynamics of Excitons in J Aggregates of a Carbocyanine Dye. *J. Chem. Phys.* **1995**, *102*, 6362–6370.

45. Augulis, R.; Pugzlys, A.; van Loosdrecht, P. H. M. Exciton Dynamics in Molecular Aggregates. *Phys. Status Solidi C* **2006**, *3*, 3400–3403.

46. Sperling, J.; Nemeth, A.; Hauer, J.; Abramavicius, D.; Mukamel, S.; Kauffmann, H. F.; Milota, F. Excitons and Disorder in Molecular Nanotubes: A 2D Electronic Spectroscopy Study and First Comparison to a Microscopic Model. *J. Phys. Chem. A* **2010**, *114*, 8179–8189.

47. Milota, F.; Sperling, J.; Nemeth, A.; Kauffmann, H. Two-Dimensional Electronic Photon Echoes of a Double Band J-Aggregate: Quantum Oscillatory Motion versus Exciton Relaxation. *Chem. Phys.* **2009**, *357*, 45–53.

48. Womick, J. M.; Miller, S. A.; Moran, A. M. Probing the Dynamics of Intraband Electronic Coherences in Cylindrical Molecular Aggregates. *J. Phys. Chem. A* **2009**, *113*, 6587–6598.

49. Womick, J. M.; Miller, S. A.; Moran, A. M. Correlated Exciton Fluctuations in Cylindrical Molecular Aggregates. *J. Phys. Chem. B* **2009**, *113*, 6630–6639.

50. Stone, K. W.; Gundogdu, K.; Turner, D. B.; Li, X.; Cundiff, S. T.; Nelson, K. A. Two-Quantum 2D FT Electronic Spectroscopy of Biexcitons in GaAs Quantum Wells. *Science* **2009**, *324*, 1169–1173.

51. Ruetzel, S.; Kullmann, M.; Buback, J.; Nuernberger, P.; Brixner, T. Tracing the Steps of Photoinduced Chemical Reactions in Organic Molecules by Coherent Two-Dimensional Electronic Spectroscopy Using Triggered Exchange. *Phys. Rev. Lett.* **2013**, *110*, 148305.

52. Shabani, A.; Kosut, R. L.; Mohseni, M.; Rabitz, H.; Broome, M. A.; Almeida, M. P.; Fedrizzi, A.; White, A. G. Efficient Measurement of Quantum Dynamics *via* Compressive Sensing. *Phys. Rev. Lett.* **2011**, *106*, 100401.

53. Sanders, J. N.; Saikin, S. K.; Mostame, S.; Andrade, X.; Widom, J. R.; Marcus, A. H.; Aspuru-Guzik, A. Compressed Sensing for Multidimensional Spectroscopy Experiments. *J. Phys. Chem. Lett.* **2012**, *3*, 2697–2702.

54. Cerullo, G.; De Silvestri, S. Ultrafast Optical Parametric Amplifiers. *Rev. Sci. Instrum.* **2003**, *74*, 1–18.